Co$_3$O$_4$@CoS Core-Shell Nanosheets on Carbon Cloth for High Performance Supercapacitor Electrodes

Jinfeng Ning [1], Tianyu Zhang [1], Ying He [1,*], Congpu Jia [1], Petr Saha [2] and Qilin Cheng [1,2,*]

[1]   Key Laboratory for Ultrafine Materials of Ministry of Education, School of Materials Science and Engineering, East China University of Science and Technology, Shanghai 200237, China; ningjinfeng0202@163.com (J.N.); tianyu.zhang1994@gmail.com (T.Z.); congpujia@163.com (C.J.)
[2]   Centre of Polymer Systems, Tomas Bata University in Zlin, nam. T. G. Masaryka 5555, Zlin 760 01, Czech Republic; saha@utb.cz
*   Correspondence: rehey@ecust.edu.cn (Y.H.); chengql@ecust.edu.cn (Q.C.)

Abstract: In this work, a two-step electrodeposition strategy is developed for the synthesis of core-shell Co$_3$O$_4$@CoS nanosheet arrays on carbon cloth (CC) for supercapacitor applications. Porous Co$_3$O$_4$ nanosheet arrays are first directly grown on CC by electrodeposition, followed by the coating of a thin layer of CoS on the surface of Co$_3$O$_4$ nanosheets via the secondary electrodeposition. The morphology control of the ternary composites can be easily achieved by altering the number of cyclic voltammetry (CV) cycles of CoS deposition. Electrochemical performance of the composite electrodes was evaluated by cyclic voltammetry, galvanostatic charge–discharge and electrochemical impedance spectroscopy techniques. The results demonstrate that the Co$_3$O$_4$@CoS/CC with 4 CV cycles of CoS deposition possesses the largest specific capacitance 887.5 F·g^{-1} at a scan rate of 10 mV·s^{-1} (764.2 F·g^{-1} at a current density of 1.0 A·g^{-1}), and excellent cycling stability (78.1% capacitance retention) at high current density of 5.0 A·g^{-1} after 5000 cycles. The porous nanostructures on CC not only provide large accessible surface area for fast ions diffusion, electron transport and efficient utilization of active CoS and Co$_3$O$_4$, but also reduce the internal resistance of electrodes, which leads to superior electrochemical performance of Co$_3$O$_4$@CoS/CC composite at 4 cycles of CoS deposition.

Keywords: Co$_3$O$_4$; CoS; carbon cloth; supercapacitor; nanostructured arrays

1. Introduction

Today, the rapidly growing global economy has caused serious energy and environmental problems which significantly influence the development and progress of human society. Consequently, the search for sustainable and clean energy as well as efficient energy conversion and storage technologies becomes imperative [1]. Among various storage systems, supercapacitors (SCs), also known as electrochemical capacitors or ultra-capacitors, have recently attracted considerable attention due to their high power density, long cycle life, good operational safety and ultrafast charge-discharge rate [2]. Although significant progress has been made in SCs so far, the energy density is still insufficient for their practical applications. The performance of SCs depends mostly on the electrochemical activity and kinetic characteristic of the electrodes. Therefore, the design and tailoring of electrode materials with satisfactory performance are of great scientific and engineering significance.

Electrode materials for SCs mainly include carbons based on electric double layer charge storage mode, metal oxides and conducting polymers based on the pseudocapacitive charge storage mechanism [3,4]. It has been shown that the pseudocapacitance is much higher than the electric double layered capacitance due to the Faradaic redox reaction on the surface of pseudocapacitive materials [5]. As a result, various metal oxides or conducting polymers used for SCs electrodes have

been investigated. Of all the metal oxides, Co_3O_4 is regarded as one of the most promising electrode materials because of its high specific capacitance, high redox reactivity, environmental friendliness and low cost [6]. However, the Co_3O_4 suffers from poor conductivity, low utilization rate, and especially low specific capacity compared to theoretical value at high current density or high scan rate, which greatly limits application when it is used as a single material [7,8]. To overcome these disadvantages, one effective strategy is to design and fabricate Co_3O_4 based composites combined with highly conductive materials such as carbonaceous materials [9–11] and conducting polymers [12–14] to improve the cycling stability and rate performance. The other strategy is integration of Co_3O_4 with metal oxides with an optimal design to enhance the electrochemical performance because of the synergistic effect between them. For instance, Cheng et al. [15] reported 3D hierarchical $Co_3O_4@MnO_2$ core-shell heterostructures grown on nickel foam exhibited an enhanced capacitance (1693.2 $F·g^{-1}$ at 1 $A·g^{-1}$), long-term cycling stability (10.2% capacitance loss after 5000 cycles) and high energy density (66.2 $Wh·kg^{-1}$ at a power density of 0.25 $kW·kg^{-1}$) with respect to that of the individual Co_3O_4 nanoneedles or MnO_2 nanosheets. Also, Gong et al. [16] developed a novel 3D nanoarchitectured $Co_3O_4@Ni(OH)_2$ core-shell electrode presented an ultrahigh areal capacitance of 15.83 $F·cm^{-1}$ with very high mass loading (11.9 $mg·cm^{-2}$). Despite considerable achievements, the challenge still remains to simultaneously achieve high capacity, good rate capability and long cycling life for Co_3O_4 based electrodes [17,18].

Recently, transition metalsulfidessuch as CoS [19–21], NiS [22,23] and MoS_2 [24] have been extensively investigated as electrode materials for SCs due to higher electrical conductivity and richer redox reactions than those of their oxide and hydroxide counterparts [25]. Thus, construction of $Co_3O_4@CoS$ nanoarchitectures with a rational design is vital for boosting electrochemical performance. In particular, core-shell nanostructured arrays on conducting substrates as bind-free electrodes combine the merits of both building blocks and porous structures [26]. As a result, fast electron/ion transfer, rich accessible electroactive sites, and easy diffusion of electrolyte might be simultaneously obtained to maximize the electrochemical performance of electrodes [27,28]. In this regard, however, few studies [29] are available on the fabrication and electrochemical properties of $Co_3O_4@CoS$ core-shell nanoplate heterostructures.

With the development of flexible electronics, lightweight and flexible/bendable substrates are required for practical applications. Conventional metal substrates (e.g., nickel foam, stainless steel mesh) used as a current collector inevitably increase weight of the total devices, which significantly weakened the energy density per total weight of the devices. As one of the most fascinating substrates, carbon cloth (CC) consists of a network of micro sized carbon fibers have been used as a scaffold for deposition of various active materials due to its large surface area, high physical strength, low sheet resistance, and flexible feature [30,31]. However, it is still a challenge to rationally design and fabricate $Co_3O_4@CoS$ core-shell structure on CC with superior electrochemical performance by using an efficient synthetic method.

Herein, we develop a two-step electrodeposition approach to construct a 3D $Co_3O_4@CoS$ core-shell nanosheet arrays grown on CC as a binder-free electrode for high-performance supercapacitor. Co_3O_4 nanosheet arrays are first directly grown on carbon cloth by electrodeposition, then CoS nanoparticles are electrodeposited on the surface of Co_3O_4 to form composite arrays. The as-prepared CC supported $Co_3O_4@CoS$ composites exhibit excellent performance, such as high specific capacitances of 887.5 $F·g^{-1}$ at a scan rate of 10 $mV·s^{-1}$ and 764.2 $F·g^{-1}$ at a current density of 1.0 $A·g^{-1}$, and long-term cycling stability (78.1% capacitance retention) at 5.0 $A·g^{-1}$ after 5000 cycles. In addition, the morphologies control of $Co_3O_4@CoS/CC$ and relationship between the electrode structure and electrochemical properties are also discussed in detail.

2. Experimental

2.1. Synthesis of Co₃O₄/CC and CoS/CC Composites

A commercially available CC (WOS1002, CeTech Co., Ltd., Taiwan) was used as the collector and supporting substrate for the final composites. Before the experiment, five pieces of carbon cloth (2 cm × 1 cm) were treated with 10 mL aqua regia for 6 h at room temperature to remove impurities. All electrodeposition experiments were performed on an electrochemical workstation (CHI 660E, CH instruments Inc., Shanghai, China) with a standard three-electrode cell, where a CC was the working electrode, a platinum plate and an Ag/AgCl were used as the counter electrode and reference electrode, respectively. Co_3O_4 nanosheets were successfully grown on the treated CC substrate via a simple electrodeposition reaction and followed by an annealing treatment. In a typical process, $Co(OH)_2$ precursor was electrodeposited in a 0.05 M $Co(NO_3)_2$ aqueous solution with 5% DMSO (dimethylsulfoxide). The deposition potential was –1.0 V (vs. Ag/AgCl). After 400 s of electrochemical reaction (the influence of the deposition time on surface morphology and the resulting performance of Co_3O_4 on carbon cloth (CC) are shown in Figures S1 and S2), the precursor was carefully washed several times with deionized water and absolute ethanol with ultrasonication, and then dried in a vacuum oven at 60 °C. Finally, the sample was calcined at 400 °C for 3 h with a heating rate of 3 °C·min^{-1} to convert to Co_3O_4 nanosheets.

CoS/CC composite was also obtained by electrodeposition. The reaction was performed in 0.05 M $CoCl_2 \cdot 6H_2O$ and 1.0 M thiourea mixed aqueous solution. The potential interval was set between -1.2 V and 0.2 V at a scan rate of 5 mV·s^{-1}. The sample was produced by 4 CV cycles of CoS deposition. Finally, it was washed with ethanol and distilled water several times, and then dried in the vacuum oven at 60 °C.

2.2. Synthesis of Co₃O₄@CoS/CC Composites

The as-prepared Co_3O_4/CC composite acted as the working electrode. Compared to the potentiostatic electrodeposition processes, the CoS layer can be much more uniform and relatively more porous after cyclic voltammetry (CV) deposition [32]. Therefore, the thin layer of CoS particles coated on Co_3O_4/CC were carried out by CV on the electrochemical workstation in 0.05 M $CoCl_2 \cdot 6H_2O$ and 1.0 M thiourea mixed aqueous solution. The potential interval was set between -1.2 V and 0.2 V at a scan rate of 5.0 mV·s^{-1}. The amount of CoS loading on the surface of Co_3O_4 was controlled by the number of CV cycles of CoS electrodeposition. The number of CV cycles of CoS deposition was kept at 1, 2, 3, 4, and 5, respectively. Afterwards, all the samples were washed with ethanol and distilled water several times, and then dried in the vacuum oven at 60 °C.

2.3. Materials Characterization

The morphology and structure of materials were tested by a field-emission scanning electron microscope (FESEM, S-4800, HITACHI, Tokyo, Japan). The chemical components of the composites were examined by X-ray photoelectron spectroscopy (XPS, ESCLAB250Xi, Thermo Scientific, Waltham, MA, USA). The structure of the samples was determined by X-ray diffraction (XRD, Cu Kα irradiation; $\lambda = 1.5418 \AA$) with a Siemens D5000 X-ray diffractometer. Raman spectra (Gloucestershire, UK) were measured with a 531.4 nm laser as the excitation source on an Acton Raman spectrometer. X-ray photoelectron spectroscopy (XPS) was collected on an AXIS Ultra DLD spectrometer (Kratos Analytical Ltd., Manchester, UK) using a monochromatized Al Kα X-ray source (1486.71 eV).

2.4. Electrochemical Measurements

The electrochemical measurements were carried out in a three-electrode testing system (CHI 660). The Co_3O_4@CoS/CC nanocomposites were used as the working electrode, an Ag/AgCl electrode and a platinum electrode were regarded as reference electrodes and counter electrodes, respectively. 1 M

KOH solution was used as the electrolyte during the electrochemical reaction. Cyclic voltammetry (CV) and galvanostatic charge–discharge (GCD) curves were recorded from −0.1 to 0.5 V. The electrochemical impedance spectroscopy (EIS) were tested in the frequency from 0.01 to 100 kHz. The specific capacitance calculated from the CV curves and discharge curves can be derived from the Equations (1) and (2), respectively:

$$\mathrm{C} = \frac{\int I \cdot dV}{m \cdot v \cdot \Delta V} \tag{1}$$

$$\mathrm{C} = \frac{I \cdot \Delta t}{m \cdot \Delta V} \tag{2}$$

where I (A) is the response of current, m (g) is the mass of the active materials in the electrode, v (V s^{-1}) is the scan rate, Δt refers to the discharge time and ΔV (V) is the potential window. The loading mass of active materials on the electrode is around 2.06 mg.

3. Results and Discussion

3.1. Morphology and Structural Characterization

The preparation process of ordered Co_3O_4@CoS nanosheet arrays on the CC via a two-step electrodeposition method is schematically illustrated in Figure 1. Typically, $Co(OH)_2$ was first electrodeposited on CC in a $Co(NO_3)_2$ aqueous solution, followed by a calcination process resulting in dense arrays of Co_3O_4 nanosheets grown vertically on the CC substrate; The reaction equations of Co_3O_4 formation process can be described as follows [33]:

$$NO_3^- + 7H_2O + 8e^- \rightarrow NH_4^+ + 10OH^- \tag{3}$$

$$Co^{2+} + 2OH^- \rightarrow Co(OH)_2 \tag{4}$$

$$Co(OH)_2 \rightarrow CoO + H_2O \tag{5}$$

$$6CoO + O_2 \rightarrow 2Co_3O_4 \tag{6}$$
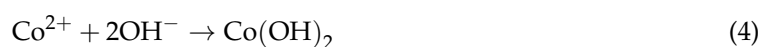
Subsequently, the as-synthesized Co_3O_4 nanosheets were coated with a thin layer of CoS particles by a controllable electrochemical deposition process to form hierarchical ternary nanocomposite. Both Co_3O_4 and CoS are employed as active materials, while the conductive CC as a current collector guarantees effective ion and electron transport throughout the electrode [34].
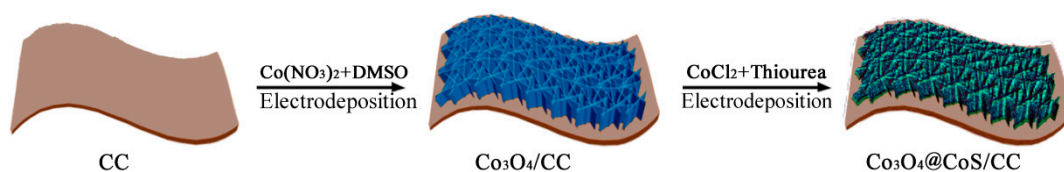

Figure 1. Schematic illustration of the two-step synthesis of Co_3O_4@CoS core-shell nanosheet arrays on carbon cloth (CC).

The morphologies of porous Co_3O_4 nanosheet arrays and CoS-coated Co_3O_4 nanosheet arrays on CC were investigated by SEM and the results are presented in Figure 2. As shown in Figure 2a, the dense Co_3O_4 nanosheets almost grew vertically on the surface of CC. The nanosheets have an edge length of 400–500 nm and a thickness of less than 10 nm. The assembly of these sheets forms a hierarchical porous structure to facilitate penetration of electrolyte ions into the inner of electrode materials. The CoS/CC composite also exhibits the similar flake-like shape on CC (Figure 2a, inset). The surface morphology of Co_3O_4@CoS/CC composite with 1–5 CV cycles of CoS electrodeposition is shown in Figure 2b–f. The Co_3O_4 nanosheets serve as the second electrodeposition backbone for CoS particles deposition to form the core-shell nanostructures on CC. It is obvious that the smooth surface

of the Co_3O_4 nanosheet become rough because of CoS deposition, and the thickness of nanosheets is increased to ~30 nm (Figure 2b). The composite still retains the same array structures as Co_3O_4/CC. With an increase in the CV cycles of CoS deposition (i.e., increase in the deposition time), it can be observed that the thickness of composite nanosheets gradually increases due to a growing amount of CoS loading on Co_3O_4 nanosheets (Figure 2c–e). The loading of Co_3O_4 on CC is about 1.06 mg, the weight gain before and after the deposition of CoS on Co_3O_4 /CC is the mass loading of CoS particles. With the CV cycle from 1 to 4, the mass loading of CoS increases from 0.4 to 1.0 mg. However, upon further increasing the cycles of electrodeposition, the interspaces between nanosheets are largely covered by agglomerated CoS particles (Figure 2f), which might reduce the utilization of both Co_3O_4 and CoS during the electrochemical reaction.
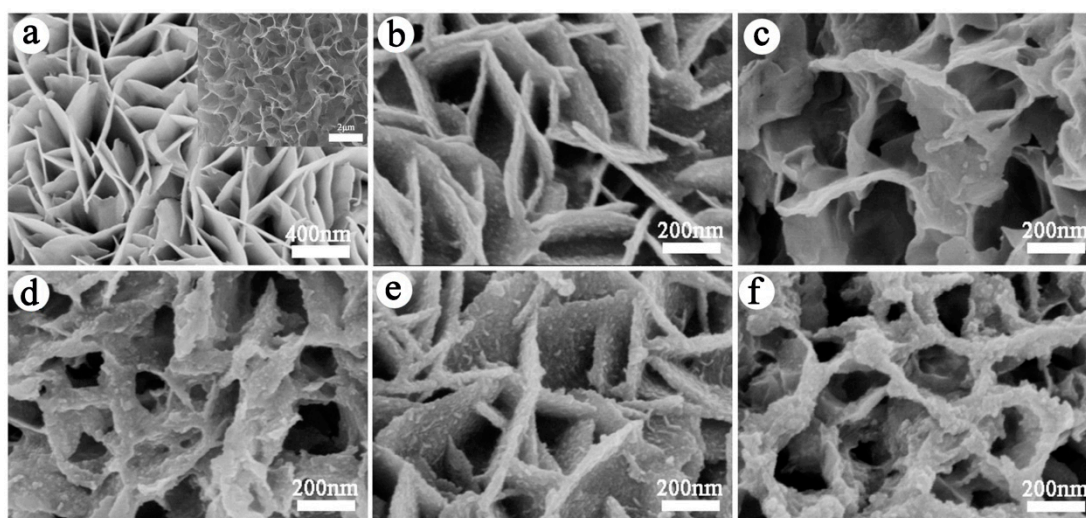

Figure 2. SEM images of (**a**) Co_3O_4/CC, inset: CoS/CC; (**b–f**) Co_3O_4@CoS/CC at 1, 2, 3, 4, 5 cycles electrodeposition, respectively.

The phase and structures of CC and CC based composites were confirmed by X-ray diffraction (XRD) and Raman spectra. As shown in Figure 3a, the XRD pattern of the CC displays two peaks at 2θ around 25° and 43° corresponding to the (002) and (100) planes of graphitic carbon, respectively. Four obvious peaks appear in the XRD pattern of Co_3O_4/CC are ascribed to cubic spinel Co_3O_4 structure phase of space group Fd3m (JCPDS No. 42-1467). After electrodeposition of CoS particles on Co_3O_4/CC, the new peaks at 2θ around 29.9°, 43.6°, 53.2° and 56.8° corresponding to (100), (102), (110), and (103) planes of CoS (JCPDS No. 65-0407) are observed in the XRD pattern of the ternary composite. The above results confirm the existence of Co_3O_4 and CoS in the ternary composite. In order to further study the structure of as-prepared composites, Raman spectra are carried out as shown in Figure 3b. The spectrum of the pure CC shows two characteristic peaks at 1343 and 1590 cm^{-1}, corresponding to the broad D and G bands of CC [35], respectively. After growth of Co_3O_4@CoS core-shell nanosheets on CC, the peaks detected at around 468 cm^{-1}, 512 cm^{-1}, 606 cm^{-1}, and 678 cm^{-1} are assigned to the E_g, F_{2g}^1, F_{2g}^2, and A_g^1 modes of Co_3O_4 [36]. Other peaks at 473 cm^{-1}, 518 cm^{-1}, and 679 cm^{-1} are referred to the E_g, F_{2g} and A_g^1 modes of CoS [37].

To verify the surface compositions of Co_3O_4@CoS/CC composite, XPS analysis was employed to characterize the sample. The XPS spectrum (Figure 4a) indicates the existence of C, O, Co and S elements in the ternary composite. High-resolution spectra of Co 2p, S 2p and O 1s are given in Figure 4b–d, respectively. As shown in Figure 4b, two major peaks and two satellite peaks are clearly presented in the XPS spectrum of Co 2p. The peak at 781.5 eV is related to Co $2p_{3/2}$, while the peak at 796.5 eV is assigned as Co $2p_{1/2}$. The energy difference between peaks of Co $2p_{1/2}$ and Co $2p_{3/2}$ is around 15 eV, indicating the presence of Co^{2+} and Co^{3+} [38]. Figure 4c shows the S 2p

spectra with the obvious peaks at 166.5 and 161.1 eV. A binding energy of approximately 166.5 eV is a typical characteristic of S^{2-} in the composite [39]. The high-resolution XPS spectrum for O 1s in Figure 4d shows the peak at 531.3 and 530.4 eV, which is attributed to the adsorptive and lattice oxygen within Co_3O_4 [40]. The above XPS results identify the co-existence of Co_3O_4 and CoS in the ternary composites.
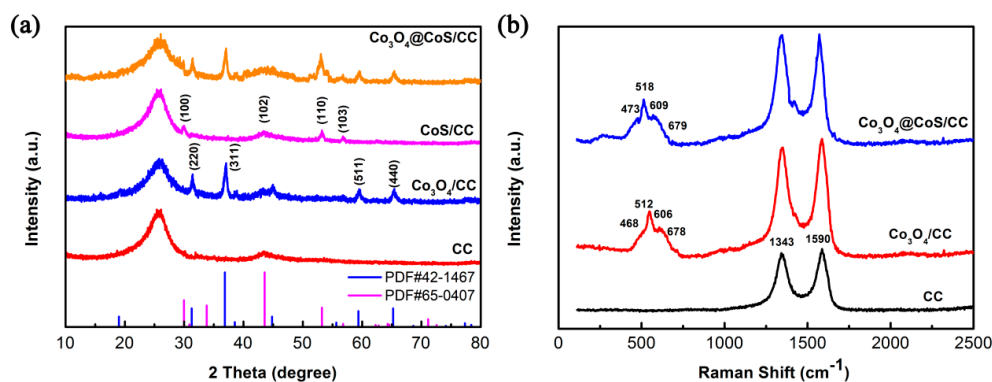

Figure 3. (**a**) XRD patterns; and (**b**) Raman spectra of CC and CC based composites.
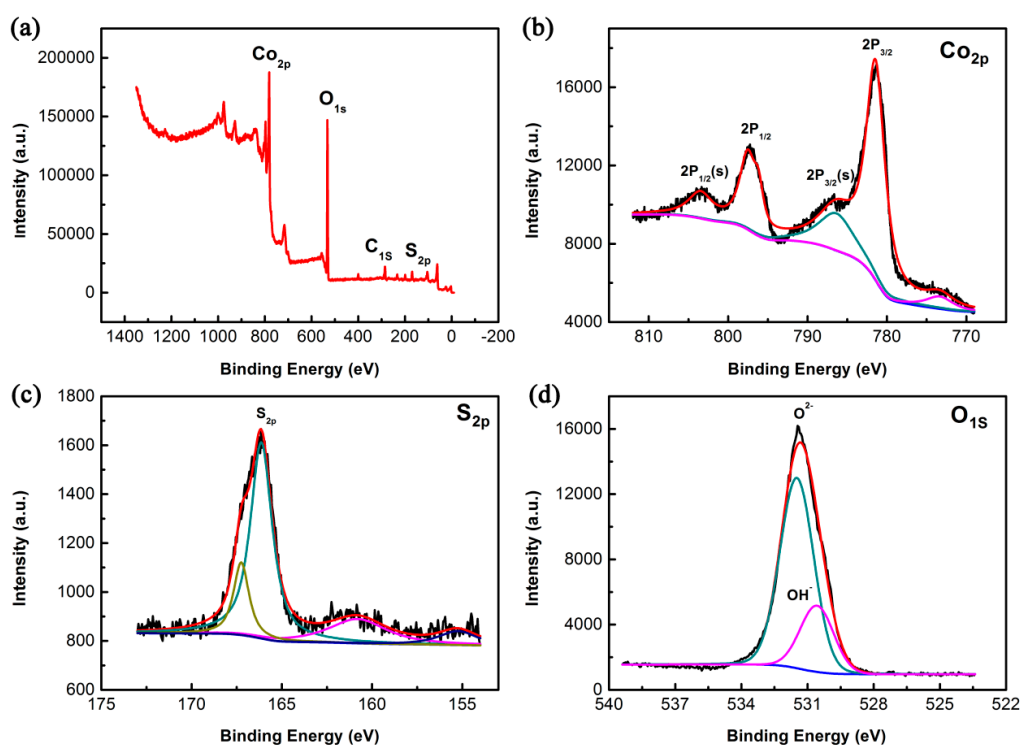
Figure 4. (**a**) XPS survey spectra of composites; (**b–d**) high-resolution XPS survey scan of Co 2p, S 2p and O 1s regions, respectively.

3.2. Electrochemical Properties

Since the Co_3O_4@CoS/CC core-shell nanosheet arrays with porous structures can not only offer richer redox chemistry and more electrochemical active sites, but also combine the contribution from both Co_3O_4 and CoS, it is expected to exhibit excellent performance as SCs electrode materials. In order to investigate the effect of CoS deposition on the capacitive performance of the ternary composite, Co_3O_4@CoS/CC composites synthesized with different electrodeposition cycles were measured by CV and GCD techniques. Figure 5a depicts the CV profiles of the ternary Co_3O_4@CoS/CC composites

obtained at 1–5 cycles of CoS deposition at the scan rate of 10 mV·s^{-1}. It is clear that all composite electrodes exhibit a similar CV shape with a pair of redox peaks within the potential range from -0.1 to 0.5 V. This pair of peaks is mainly due to the reversible redox reaction of Co^{2+}/Co^{3+} redox couple associated with OH^{-} anions in the alkaline electrolyte, as in the case of CoS [41]. With an increase in the number of CoS electrodeposition cycles, the integral area of CV curves of composite electrodes increases to the maximum (at 4 cycles) and then decreases, indicating that Co_3O_4@CoS/CC composite at 4 cycles of CoS deposition possesses the largest specific capacitance. As the number of cycles increase to 5, the integral area of CV curve decreases greatly, i.e., the specific capacitance of the composite decreases dramatically. The decreasing trend of the capacitance with increasing CoS content can be explained by the surface of Co_3O_4 nanosheets and the open spaces between nanosheets being occupied or blocked up by the excess CoS particles, which reduces the active surface area of the composite electrode. Figure 5b presents the GCD curves of the ternary composites obtained at different cycles of CoS deposition. The longer discharge time demonstrates a larger specific capacitance; apparently, the composite obtained at 4 cycles shows the maximum capacitance. The variation tendency of capacitance is the same as the CV analysis. And the relationship between the specific capacitance (calculated from Equations (1) and (2), respectively) and cycle number of CoS deposition is plotted in Figure 5c,d. The calculating results coincide with the above conclusions from CV and GCD measurements.
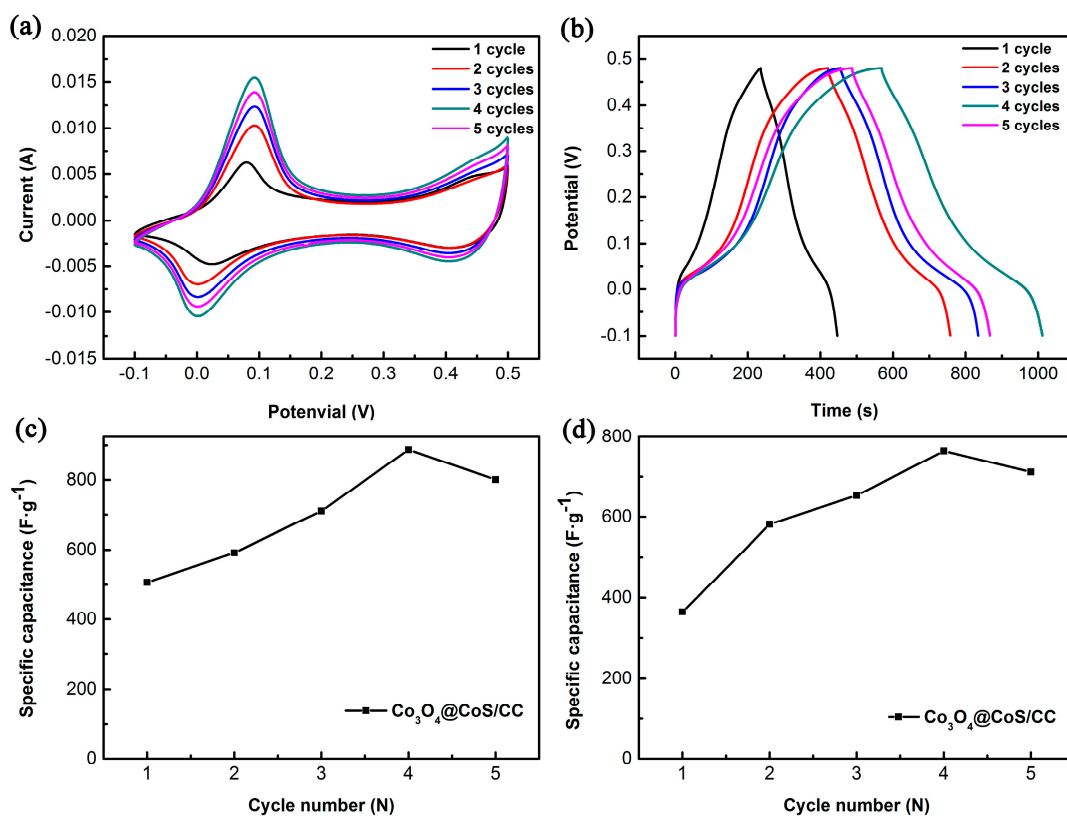

Figure 5. (**a**) CV curves of Co_3O_4@CoS/CC at different electrodeposition cycles of CoS; (**b**) Galvanostatic charge/discharge curves of Co_3O_4@CoS/CC at different electrodeposition cycles of CoS; (**c**) Specific capacitance value derived from (**a**) via cycle number of CoS deposition; (**d**) Specific capacitance value derived from (**b**) via cycle number of CoS deposition.

Since the Co_3O_4@CoS/CC composite at 4 cycles of CoS deposition exhibits the optimal capacitance, as a representative of composite electrodes, its electrochemical performance is evaluated in the following discussion. Figure 6a illustrates the CV curves of the Co_3O_4@CoS/CC composite recorded at various potential scan rates. Pairs of well-defined anodic and cathodic signals clearly appear over the

entire range of scan rates from 10–100 mV·s^{-1}. The current response increases with the increasing scan rate and all the curves show the similar shape, indicating rapid faradaic reaction between electrode and electrolyte, excellent electrochemical reversibility and high-rate performance of the Co$_3$O$_4$@CoS/CC electrode material [15]. To further evaluate the performance of the Co$_3$O$_4$@CoS/CC electrode, GCD measurements were performed at current densities of 1.0–10 A·g^{-1}. All the curves have good symmetry but deviate from a straight and flat line, suggesting that the capacitance mainly results from faradic pseudocapacitance. Even at high current density of 10 A·g^{-1}, the GCD curves have nearly symmetrical charge/discharge profiles due to the excellent interfacial contact between Co$_3$O$_4$@CoS core-shell nanostructures and carbon cloth, fast transportation of electrons and low equivalent series resistance.

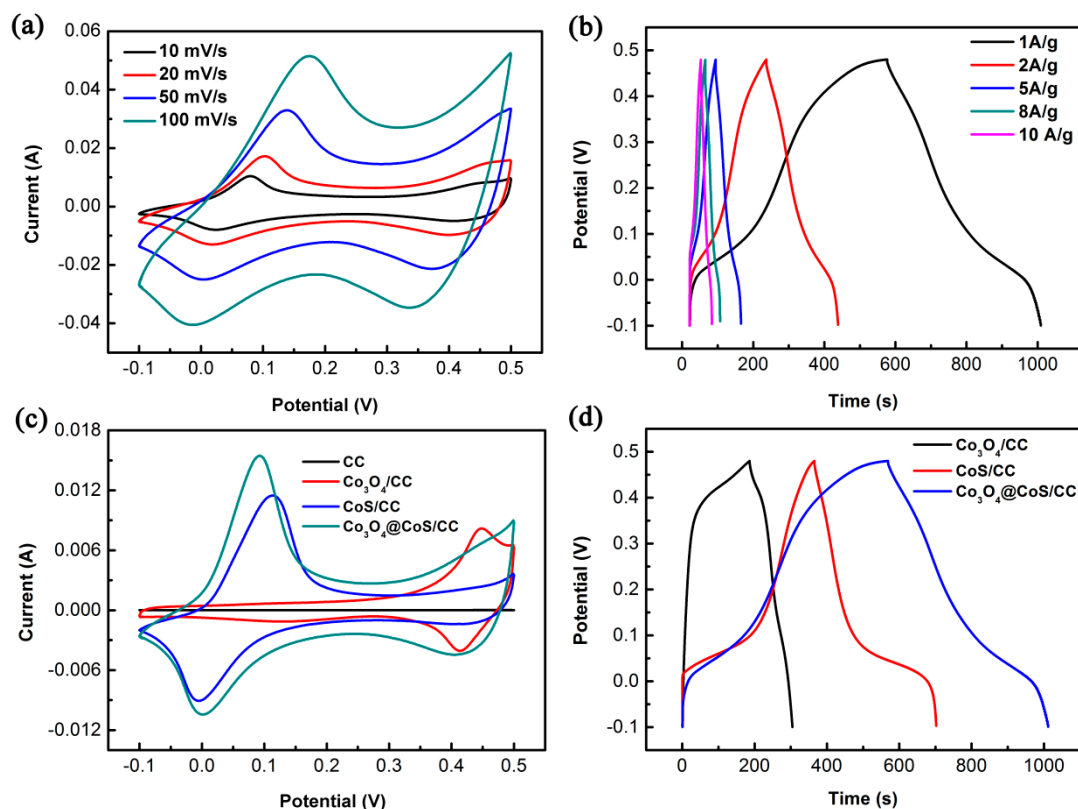**Figure 6.** (**a**) CV curves of Co$_3$O$_4$@CoS/CC at different scan rates; (**b**) Galvanostatic charge/discharge curves of Co$_3$O$_4$@CoS/CC at different current densities; (**c**) CV curves of CC, Co$_3$O$_4$/CC, CoS/CC and Co$_3$O$_4$@CoS/CC at 10 mV·s^{-1}; (**d**) Galvanostatic charge/discharge curves of Co$_3$O$_4$/CC, CoS/CC and Co$_3$O$_4$@CoS/CC at 1.0 A·g^{-1}.

To demonstrate the role of Co$_3$O$_4$ and CoS, CV curves of CC, Co$_3$O$_4$/CC, CoS/CC and Co$_3$O$_4$@CoS/CC are carried out at the same scan rate of 10 mV·s^{-1}, as shown in Figure 6c. The multiple peaks at different potentials correspond to the formation of the number of cobalt oxide phases with different oxidation states [7]. The following reversible reactions (Equations (7) and (8)) take place during the redox process.

$$Co_3O_4 + OH^- + H_2O \rightarrow 3CoOOH + e^- \tag{7}$$

$$3CoOOH + e^- \rightarrow Co_3O_4 + OH^- + H_2O \tag{8}$$
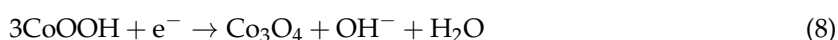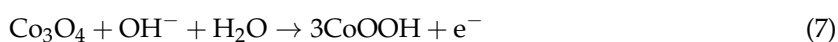
The anodic peaks (at positive current density) and cathodic peaks (at negative current density) in the CV curves are due to the oxidation and reduction processes, respectively. Two reactions of CoS are proposed for electrochemical reactions [42]:

$$CoS + OH^- \leftrightarrow CoSOH + H_2O + e^- \tag{9}$$

$$CoSOH + OH^- \leftrightarrow CoSO + H_2O + e^- \tag{10}$$
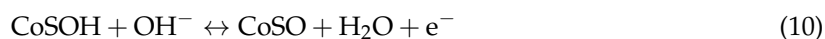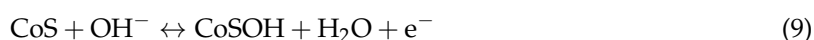
The redox peaks exist in the CV curves of the three kinds of electrode materials except for that of CC, which reflect their predominately pseudocapacitive behavior. It can be noted that the capacitance contribution of the CC substrate to the composite electrodes is very small and can be neglected owing to its very low integral area as compared to that of other composite electrodes. A comparison of the CV curves of all the composite electrodes reveals the prominent contribution of the core-shell $Co_3O_4@CoS/CC$ due to the synergistic contribution of both Co_3O_4 and CoS pseudocapacitive materials. The enclosed area increases in the following order: CC < Co_3O_4/CC < CoS/CC < $Co_3O_4@CoS/CC$, indicating that the ternary composite has the largest capacitance of both binary composites, which can be confirmed by the capacitance value calculated from Equation (1). The specific capacitance of Co_3O_4/CC, CoS/CC and $Co_3O_4@CoS/CC$ at 10 mV·s^{-1} is 295.8, 536.7, and 887.5 F·g^{-1}, respectively. Figure 6d shows the GCD curves of Co_3O_4/CC, CoS/CC and $Co_3O_4@CoS/CC$ measured at the current density of 1.0 A·g^{-1}. As expected, the ternary $Co_3O_4@CoS/CC$ composite electrode has the longest discharging time, that is, the largest specific capacitance which is calculated to be about 764.2 F·g^{-1} at 1.0 A·g^{-1}, much higher than that of Co_3O_4/CC (249.2 F·g^{-1}) and CoS/CC (581.1 F·g^{-1}). This trend of capacitance variation is consistent with CV results, which further verifies that the ternary composite electrode yields the best capacitive performance. Such a phenomenon might be due to the following reasons. First, the deposition of CoS thin layers on the Co_3O_4 nanosheets results in a boost in capacitance value. Second, the combination of CC with transition metal compounds increases the conductivity, reduces charge transfer resistance and facilitates the electron transport. Third, core-shell nanosheet arrays grown on CC with open spaces not only increase the accessible surface area for the electrochemical reaction and efficient utilization of active CoS and Co_3O_4, but they also enable easy penetration of the electrolyte into the electrode.

Rate performance of composite electrodes was also studied by GCD measurements presented in Figure 7. It is evident that the specific capacitance of all composite electrodes decreases with increasing current density because of the reduced utilization of active materials caused by the increased diffusion of ions. Note that the $Co_3O_4@CoS/CC$ ternary composite exhibit significantly higher capacitance than both binary ones over the entire current density range. The capacitance retention of the $Co_3O_4@CoS/CC$ composite can keep as much as 72.2% as the current density increases from 1.0 to 10 A·g^{-1}, while the Co_3O_4/CC and CoS/CC retain only 33.8% and 39.3% of the initial capacitance under the same condition, respectively. The enhanced rate capability of the $Co_3O_4@CoS/CC$ composite is ascribed to the advantages of its hierarchical structure. Ultrathin CoS particles layer and Co_3O_4 nanosheets with small thickness can reduce the diffusion paths for electrons/ions and facilitate fast kinetics at high charge-discharge rates, ensuring the full utilization of CoS and Co_3O_4. Meanwhile, the CC substrates act as conductive paths not only to decrease internal resistance but also to provide robust adhesion for the $Co_3O_4@CoS$ composite, and the strong synergistic effect between them also leads to improved performance.

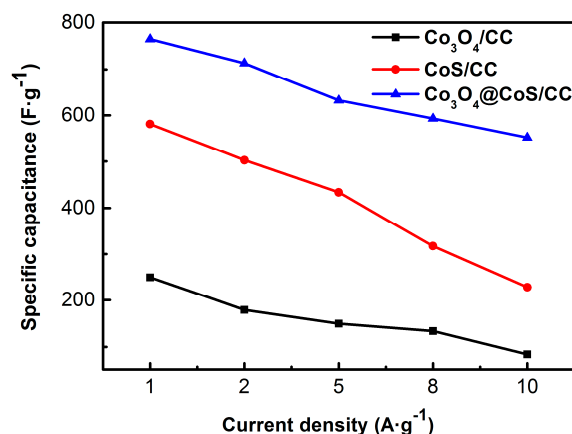**Figure 7.** Specific capacitance curves of Co_3O_4/CC, CoS/CC and Co_3O_4@CoS/CC at different current densities.

To further understand the capacitive behavior of the obtained composite electrodes, EIS were performed and the resulting Nyquist plots for Co_3O_4/CC, CoS/CC and Co_3O_4@CoS/CC electrodes are given in Figure 8a. Each electrode shows a straight line at the low-frequency region and a near semicircular shape in the high frequency region. Such a pattern of the EIS can be fitted by an equivalent circuit, as shown in the inset of Figure 8a. The intercept on the real axis represents the equivalent series resistance (R_s), and the diameter of the semicircle reflects the charge transfer resistance (R_{ct}) at the electrode/electrolyte interface [43,44]. The R_s from the Nyquist plot for Co_3O_4/CC, CoS/CC and Co_3O_4@CoS/CC electrodes is 3.29, 3.25 and 2.88 Ω, respectively, while R_{ct} for them is 7.40, 5.22 and 3.10 Ω respectively. The lowest R_s and R_{ct} of the ternary composite electrode reveal that incorporation of the CoS shell into the Co_3O_4 nanosheet arrays on CC improves the conductivity and decreases the charge-transfer resistance of the Co_3O_4@CoS/CC electrode. The redox reaction of the Co_3O_4@CoS/CC electrode mainly occurs on its surface and thus the capacitance primarily depends on the interfacial charge-transfer resistance. The lowest R_{ct} (3.1 Ω) facilitates the electron transfer and the redox reaction, thereby enhancing the capacitance. In addition, compared to both binary composite electrodes, the ternary electrode has a more vertical straight line in the low frequency range, suggesting that it has better capacitive performance due to a faster ionic diffusion rate of electrolyte ions into this ternary composite electrode. Therefore, the lower charge transfer resistance and higher ionic diffusion rate endow the Co_3O_4@CoS/CC composite with improved capacitance.
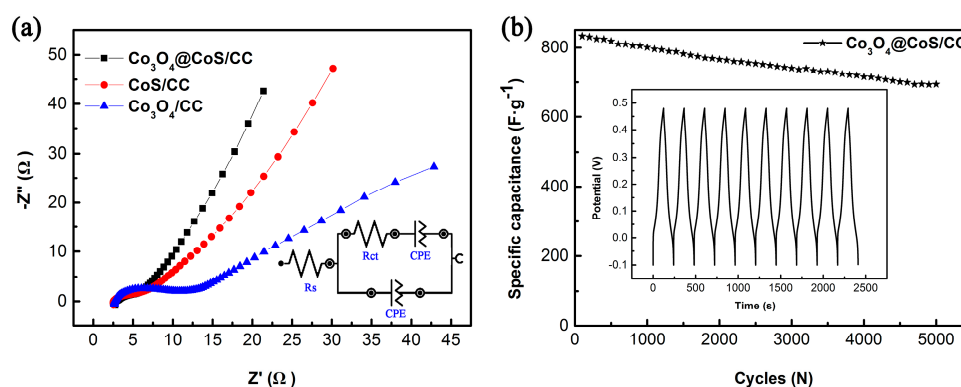

Figure 8. (**a**) electrochemical impedance spectroscopy (EIS) curves of CC, Co_3O_4/CC, and Co_3O_4@CoS/CC electrodes with insets showing the equivalent circuit diagram fitting the EIS; (**b**) Cycling stability of theCo_3O_4@CoS/CC electrode at the current density of 5 A·g^{-1} for 5000 charging-discharging cycles.

Long-term cycling stability of the ternary composite electrode is also carried out at the current density of 5.0 A·g^{-1} for 5000 cycles and the results are depicted in Figure 8b. The profiles of the charge and discharge curves exhibit a good electrochemical reversibility without perceptible deviations in each cycle, revealing good capacitive characteristics of the porous Co$_3$O$_4$@CoS/CC composite electrode. About 78.1% of its initial capacitance is retained after 5000 cycles, which is comparable to that of most Co$_3$O$_4$ or CoS based electrode materials (Table S1 and S2), indicating the superior cycling stability of the Co$_3$O$_4$@CoS/CC composite even at high current density. The above results confirm that such a rational design of Co$_3$O$_4$ and CoS on CC can maximize the electrochemical performance of composite electrode.

4. Conclusions

In summary, a facile two-step electrodeposition process has been developed for the rational design and fabrication of Co$_3$O$_4$@CoS core-shell nanostructures on CC for high-performance supercapacitor applications. The structural characterizations confirm that the thin CoS layers covered on the surface of Co$_3$O$_4$ nanosheets form 3D porous arrays on CC. A positive synergistic effect of Co$_3$O$_4$@CoS and CC endows the ternary composite with larger capacitance and better cycling stability than each individual binary composite. The as-prepared Co$_3$O$_4$@CoS/CC composite with 4 cycles of CoS deposition exhibits a high capacitance of 887.5 F·g^{-1} at 10 mV·s^{-1} and maintains 78.1% of the original capacitance after 5000 charge-discharge cycles at a large current density of 5.0 A·g^{-1}. The superior electrochemical properties highlight the importance of rational design and control of electrode structures.

Supplementary Materials: The following are available online at www.mdpi.com/1996-1944/10/6/608/s1. Figure S1: SEM images of (a) CC; (b) Co$_3$O$_4$-100s/CC; (c) Co$_3$O$_4$-200s/CC; (d) Co$_3$O$_4$-300s/CC; (e) Co$_3$O$_4$-400s/CC; (f) Co$_3$O$_4$-500s/CC; Figure S2: (a) CV curves of the Co$_3$O$_4$/CC measured at 10 mV·s^{-1}; (b) Specific capacitance of the Co$_3$O$_4$/CC measured at 10 mV·s^{-1}; (c) GCD curves of the Co$_3$O$_4$/CC measured at 1.0 A·g^{-1}; (d) Specific capacitance of the Co$_3$O$_4$/CC measured at 1.0 A·g^{-1}, Table S1: Comparison of the electrochemical performances of Co$_3$O$_4$ or CoS between literature and this study, Table S2: Comparison of the electrochemical performances and synthesis method between literature and this study.

Author Contributions: Jinfeng Ning and Tianyu Zhang conceived and designed the experiments; Jinfeng Ning and Congpu Jia performed the experiments; Ying He and Qilin Cheng analyzed the data, reviewed and edited this manuscript; Petr Saha contributed reagents/materials/analysis tools; Jinfeng Ning and Qilin Cheng wrote the paper.

Conflicts of Interest: The authors declare no conflict of interest.

References

1. Liu, C.; Li, F.; Ma, L.-P.; Cheng, H.M. Advanced materials for energy storage. *Adv. Mater.* **2010**, *22*, 28–62. [CrossRef] [PubMed]

2. Wang, Y.; Xia, Y. Recent progress in supercapacitors: From materials design to system construction. *Adv. Mater.* **2013**, *25*, 5336–5342. [CrossRef] [PubMed]

3. Hu, Q.; Gu, Z.; Zheng, X.; Zhang, X. Three-dimensional Co$_3$O$_4$@NiO hierarchical nanowire arrays for solid-state symmetric supercapacitor with enhanced electrochemical performances. *Chem. Eng. J.* **2016**, *304*, 223–231. [CrossRef]

4. Wang, G.; Zhang, L.; Zhang, J. A review of electrode materials for electrochemical supercapacitors. *Chem. Soc. Rev.* **2011**, *41*, 797–828. [CrossRef] [PubMed]

5. Shao, M.; Li, Z.; Zhang, R.; Ning, F.; Wei, M.; Evans, D.G.; Duan, X. Hierarchical conducting polymer@clay core-shell arrays for flexible all-solid-state supercapacitor devices. *Small* **2015**, *11*, 3530–3538. [CrossRef] [PubMed]

6. Xia, X.H.; Tu, J.P.; Mai, Y.J.; Wang, X.L.; Gu, C.D.; Zhao, X.B. Self-supported hydrothermal synthesized hollow Co3O4 nanowire arrays with high supercapacitor capacitance. *J. Mater. Chem.* **2011**, *21*, 9319–9325. [CrossRef]

7. Meher, S.K.; Rao, G.R. Ultra layered Co$_3$O$_4$ for high-performance supercapacitor applications. *J. Phys. Chem. C* **2011**, *115*, 15646–15654. [CrossRef]

8. Xia, X.H.; Tu, J.P.; Zhang, Y.Q.; Mai, Y.J.; Wang, X.L.; Gu, C.D.; Zhao, X.B. Freestanding Co$_3$O$_4$ nanowire array for high performance supercapacitors. *RSC Adv.* **2012**, *2*, 1835–1841. [CrossRef]

9. Silva, R.; Pereira, G.M.; Voiry, D.; Chhowalla, M.; Asefa, T. Co$_3$O$_4$ nanoparticles/cellulose nanowhiskers derived amorphous carbon nanoneedles: Sustainable materials for supercapacitors and oxygen reduction electrocatalysis. *RSC Adv.* **2015**, *5*, 49385–49391. [CrossRef]

10. Sun, G.; Ma, L.; Ran, J.; Shen, X.; Tong, H. Incorporation of homogeneous Co$_3$O$_4$ into a nitrogen-doped carbon aerogel: Via a facile in situ synthesis method: Implications for high performance asymmetric supercapacitors. *J. Mater. Chem. A* **2016**, *4*, 9542–9554. [CrossRef]

11. Ke, Q.; Tang, C.; Yang, Z.C.; Zheng, M.; Mao, L.; Liu, H.; Wang, J. 3D Nanostructure of carbon nanotubes decorated Co$_3$O$_4$ nanowire arrays for high performance supercapacitor electrode. *Electrochim. Acta* **2015**, *163*, 9–15. [CrossRef]

12. Raj, R.P.; Ragupathy, P.; Mohan, S. Remarkable capacitive behavior of a Co$_3$O$_4$-polyindole composite as electrode material for supercapacitor applications. *J. Mater. Chem. A* **2015**, *3*, 24338–24348. [CrossRef]

13. Lin, H.; Huang, Q.; Wang, J.; Jiang, J.; Liu, F.; Chen, Y.; Wang, C.; Lu, D.; Han, S. self-assembled graphene/polyaniline/Co$_3$O$_4$ ternary hybrid aerogels for supercapacitors. *Electrochim. Acta* **2016**, *191*, 444–451. [CrossRef]

14. Hong, W.; Wang, J.; Li, Z.; Yang, S. Hierarchical Co$_3$O$_4$@Au-decorated PPy core/shell nanowire arrays: An efficient integration of active materials for energy storage. *J. Mater. Chem. A* **2015**, *3*, 2535–2540. [CrossRef]

15. Kong, D.; Luo, J.; Wang, Y.; Ren, W.; Yu, T.; Luo, Y.; Yang, Y.; Cheng, C. Three-dimensional Co$_3$O$_4$@MnO$_2$ hierarchical nanoneedle arrays: Morphology control and electrochemical energy etorage. *Adv. Funct. Mater.* **2014**, *24*, 3815–3826. [CrossRef]

16. Tang, C.H.; Yin, X.; Gong, H. Superior performance asymmetric supercapacitors based on a directly grown commercial mass 3D Co$_3$O$_4$@Ni(OH)$_2$ core-shell electrode. *ACS Appl. Mater. Interfaces* **2013**, *5*, 10574–10582. [CrossRef] [PubMed]

17. Zhong, J.H.; Wang, A.L.; Li, G.R.; Wang, J.W.; Ou, Y.N.; Tong, Y.X. Co$_3$O$_4$/Ni(OH)$_2$ composite mesoporous nanosheet networks as a promising electrode for supercapacitor applications. *J. Mater. Chem.* **2012**, *22*, 5656–5665. [CrossRef]

18. Zhang, G.; Wang, T.; Yu, X.; Zhang, H.; Duan, H.; Lu, B. Nanoforest of hierarchical Co$_3$O$_4$@NiCo$_2$O$_4$ nanowire arrays for high-performance supercapacitors. *Nano Energy* **2013**, *2*, 586–594. [CrossRef]

19. Li, S.; Wen, J.; Chen, T.; Xiong, L.; Wang, J.; Fang, G. In situ synthesis of 3D CoS nanoflake/Ni(OH)$_2$ nanosheet nanocomposite structure as a candidate supercapacitor electrode. *Nanotechnology* **2016**, *27*, 1–9.

20. Luo, F.; Li, J.; Yuan, H.; Xiao, D. Rapid synthesis of three-dimensional flower-like cobalt sulfide hierarchitectures by microwave assisted heating method for high-performance supercapacitors. *Electrochim. Acta* **2014**, *123*, 183–189. [CrossRef]

21. Ray, R.S.; Sarma, B.; Jurovitzki, A.L.; Misra, M. Fabrication and characterization of titania nanotube/cobalt sulfide supercapacitor electrode in various electrolytes. *Chem. Eng. J.* **2015**, *260*, 671–683. [CrossRef]

22. Wang, A.; Wang, H.; Zhang, S.; Mao, C.; Song, J.; Niu, H.; Jin, B.; Tian, Y. Controlled synthesis of nickel sulfide/graphene oxide nanocomposite for high-performance supercapacitor. *Appl. Surf. Sci.* **2013**, *282*, 704–708. [CrossRef]

23. Wu, J.; Ouyang, C.; Dou, S.; Wang, S. Hybrid NiS/CoO mesoporous nanosheet arrays on Ni foam for high-rate supercapacitors. *Nanotechnology* **2015**, *26*, 1–8. [CrossRef] [PubMed]

24. Javed, M.S.; Dai, S.; Wang, M.; Guo, D.; Chen, L.; Wang, X.; Hu, C.; Xi, Y. High performance solid state flexible supercapacitor based on molybdenum sulfide hierarchical nanospheres. *J. Power Sourous* **2015**, *285*, 63–69. [CrossRef]

25. Yu, X.Y.; Yu, L.; Shen, L.; Song, X.; Chen, H.; Lou, X.W. General formation of MS (M = Ni, Cu, Mn) box-in-box hollow structures with enhanced pseudocapacitive properties. *Adv. Funct. Mater.* **2014**, *24*, 7440–7446. [CrossRef]

26. Wang, H.Y.; Xiao, F.X.; Yu, L.; Liu, B.; Lou, X.W. Hierarchical α-MnO$_2$ nanowires@Ni$_{1-x}$Mn$_x$O$_y$ nanoflakes core-shell nanostructures for supercapacitors. *Small* **2014**, *10*, 3181–3186. [CrossRef] [PubMed]

27. Wang, X.; Lu, X.; Liu, B.; Chen, D.; Tong, Y.; Shen, G. Flexible energy-storage devices: Design consideration and recent progress. *Adv. Mater.* **2014**, *26*, 4763–4782. [CrossRef] [PubMed]

28. Xu, J.; Wang, K.; Zu, S.Z.; Han, B.H.; Wei, Z. Hierarchical nanocomposites of polyaniline nanowire arrays on graphene oxide sheets with synergistic effect for energy storage. *ACS Nano* **2010**, *4*, 5019–5026. [CrossRef] [PubMed]

29. Liu, B.; Kong, D.; Zhang, J.; Wang, Y.; Chen, T.; Cheng, C.; Yang, H.Y. 3D hierarchical Co_3O_4@Co_3S_4 nanoarrays as cathode materials for asymmetric pseudocapacitors. *J. Mater. Chem. A* **2016**, *4*, 3287–3296. [CrossRef]

30. Zhang, L.; Huang, T.J.; Gong, H. Remarkable improvement in supercapacitor performance by sulfur introduction during a one-step synthesis of nickel hydroxide. *Phys. Chem. Chem. Phys.* **2017**, *19*, 10462–10469. [CrossRef] [PubMed]

31. Yang, L.; Cheng, S.; Ding, Y.; Zhu, X.; Wang, Z.L.; Liu, M. Hierarchical network architectures of carbon fiber paper supported cobalt oxide nanonet for high-capacity pseudocapacitors. *Nano Lett.* **2012**, *12*, 321–325. [CrossRef] [PubMed]

32. Li, R.; Wang, S.; Wang, J.; Huang, Z. N_3S_2@CoS core-shell nano-triangular pyramid arrays on Ni foam for high-performance supercapacitors. *Phys. Chem. Chem. Phys.* **2015**, *17*, 16434–16442. [CrossRef] [PubMed]

33. Li, X.; Guan, G.; Du, X.; Jagadale, A.D.; Cao, J.; Hao, X.; Ma, X.; Abudula, A. Homogeneous nanosheet Co_3O_4 film prepared by novel unipolar pulse electro-deposition method for electrochemical water splitting. *RSC Adv.* **2015**, *5*, 76026–76031. [CrossRef]

34. Li, H.; He, Y.; Pavlinek, V.; Cheng, Q.; Saha, P.; Li, C. MnO_2 nanoflake/polyaniline nanorod hybrid nanostructures on graphene paper for high-performance flexible supercapacitor electrodes. *J. Mater. Chem. A* **2015**, *3*, 17165–17171. [CrossRef]

35. Kim, C.; Yang, K.; Kojima, M.; Yoshida, K.; Kim, Y.J.; Kim, Y.A.; Endo, M. Fabrication of electrospinning-derived carbon nanofiber webs for the anode material of lithium-ion secondary batteries. *Adv. Funct. Mater.* **2006**, *16*, 2393–2397. [CrossRef]

36. Dong, X.C.; Xu, H.; Wang, X.W.; Huang, Y.X.; Chan-Park, M.B.; Zhang, H.; Wang, L.H.; Huang, W.; Chen, P. 3D graphene–cobalt oxide electrode for high-performance supercapacitor and enzymeless glucose detection. *ACS Nano* **2012**, *6*, 3206–3213. [CrossRef] [PubMed]

37. Hadjiev, V.G.; Iliev, M.N.; Vergilov, I.V. The Raman spectra of Co_3O_4. *J. Phys. C Solid State Phys.* **1988**, *21*, 199–201. [CrossRef]

38. Xu, J.; Fu, G.; Tang, Y.; Zhao, T.S. Non-precious Co_3O_4 nano-rod electrocatalyst for oxygen reduction reaction in anion-exchange membrane fuel cells. *Energy Environ. Sci.* **2012**, *5*, 5333–5339. [CrossRef]

39. Sun, H.; Qin, D.; Huang, S.; Guo, X.; Li, D.; Luo, Y.; Meng, Q. Dye-sensitized solar cells with NiS counter electrodes electrodeposited by a potential reversal technique. *Energy Environ. Sci.* **2011**, *4*, 2630–2637. [CrossRef]

40. Mate, V.R.; Shirai, M.; Rode, C.V. Heterogeneous Co_3O_4, catalyst for selective oxidation of aqueous veratryl alcohol using molecular oxygen. *Catal. Commun.* **2013**, *33*, 66–69. [CrossRef]

41. Tao, F.; Zhao, Y.Q.; Zhang, G.Q.; Li, H.L. Electrochemical characterization on cobalt sulfide for electrochemical supercapacitors. *Electrochem. Commun.* **2007**, *9*, 1282–1287. [CrossRef]

42. Chen, C.Y.; Shih, Z.Y.; Yang, Z.; Chang, H.T. Carbon nanotubes/cobalt sulfide composites as potential high-rate and high-efficiency supercapacitors. *J. Power Sourous* **2012**, *215*, 43–47. [CrossRef]

43. Huang, C.W.; Teng, H. Influence of carbon nanotube grafting on the impedance behavior of activated carbon capacitors. *J. Electrochem. Soc.* **2008**, *155*, 739–744. [CrossRef]

44. Li, W.; Li, G.; Sun, J.; Zou, R.; Xu, K.; Sun, Y.; Chen, Z.; Yang, J.; Hu, J. Hierarchical heterostructures of MnO_2 nanosheets or nanorods grown on Au-coated Co_3O_4 porous nanowalls for high-performance pseudocapacitance. *Nanoscale* **2013**, *5*, 2901–2908. [CrossRef] [PubMed]